Earth and Planetary Science Letters 285 (2009) 39–51

Contents lists available at ScienceDirect

Earth and Planetary Science Letters

journal homepage: www.elsevier.com/locate/epsl

# Magneto-biostratigraphy of the Cicogna section (Italy): Implications for the late Paleocene–early Eocene time scale

Edoardo Dallanave [a,b,*], Claudia Agnini [a], Giovanni Muttoni [b,c], Domenico Rio [a]

[a] Department of Geosciences, University of Padova, Via Giotto 1, I-35137 Padova, Italy
[b] ALP – Alpine Laboratory of Paleomagnetism, Via Madonna dei Boschi 76, I-12016 Peveragno (CN), Italy
[c] Department of Earth Sciences, University of Milan, Via Mangiagalli, 34 I-20133 Milano, Italy

ARTICLE INFO

*Article history:*
Received 26 January 2009
Received in revised form 21 April 2009
Accepted 22 May 2009
Available online 24 June 2009

Editor: P. DeMenocal

*Keywords:*
paleocene
eocene
magnetostratigraphy
biostratigraphy
magnetic properties
chronology

ABSTRACT

We present the magnetostratigraphy and calcareous nannofossil biostratigraphy of the ~81 m thick upper Paleocene–lower Eocene Cicogna section from the Belluno Basin of NE Italy. The Cicogna section extends in stratigraphic continuity from Chron C25r to Chron C23r and from nannofossil Zone NP7/NP8 to NP12 (=CP6–CP10), thus covering an interval of time comprised between ~56.6 and ~52.2 Ma. Inferred sediment accumulation rates were relatively constant in the order of ~18 m/Myr, and were used to estimate the age of standard calcareous nannofossil events for comparison with, and improvements of, current time scales. We found several new and potentially useful biohorizons that help refining the chronology of this critical interval of time encompassing a long and biochronologically poorly known Chron C24r. We furthermore observed an apparent correlation between rock-magnetic properties of the sediments and global climate variability as revealed by a reference benthic $\delta^{18}O$ record from the literature, whereby higher relative amounts of oxidized magnetic phases such as hematite and/or maghemite seem to correlate to extreme warm periods like the PETM at ~55 Ma and the early Eocene from ~54 to ~52.5 Ma. Mechanisms able to explain this apparent coupling between rock-magnetic variability and long-term global climate are presently under scrutiny.
© 2009 Elsevier B.V. All rights reserved.

## 1. Introduction

During the late Paleocene–early Eocene, the Earth experienced a global warming trend that culminated in the early Eocene climatic optimum (EECO; e.g. Zachos et al., 2001), characterized by warm climate conditions at even extreme high latitudes (McKenna, 1980; Moran et al., 2006), subdued latitudinal temperature gradients (Wolfe, 1980; Estes and Hutchison, 1980; Axelrod, 1984), and virtually nonexistent polar ice sheets (Wise et al., 1991; Zachos et al., 1994). This warming trend was punctuated by several short-lived hyperthermal events (Cramer et al., 2003), the most prominent of which was the Paleocene Eocene thermal maximum (PETM; e.g. Kennett and Stott, 1991).

The magneto-biochronology of this critical time interval is however still poorly defined, essentially because of the controversial and ambiguous relationships between paleontologic and magnetic events due to the presence of unconformities in several deep-sea and shallow water sections from the literature around the Paleocene–Eocene boundary (e.g. DSDP Sites 549 and 550) (Aubry et al., 1996), and the lack of (magnetic) resolution in the long Chron C24r interval (Berggren et al., 1995 and references therein).

We present the magnetostratigraphy and calcareous nannofossil biostratigraphy of the upper Paleocene–lower Eocene Cicogna section from the Venetian Southern Alps (NE Italy). The Cicogna section consists of ~81 m of continuously exposed marine marlstones, with no apparent variations in sediment accumulation rates, and thus offers the possibility to assess in detail the magneto-biochronology of this time interval for comparison with, and potential improvement of, the current reference time scale of Berggren et al. (1995, hereafter referred to as BKSA95). An assessment of the rock-magnetic content of the section is also presented and used in conjunction with benthic oxygen isotope data from the literature to put forward a speculative model of climate-controlled rock-magnetic variability over the late Paleocene–early Eocene, which will be extensively developed in a parallel paper in preparation.

## 2. Geological setting

The Venetian Southern Alps consist of a series of paleogeographic domains that developed since the Early Jurassic, namely the Trento Plateau, the Belluno Basin, and the Friuli Platform (Fig. 1) (e.g. Gaetani and Jadoul, 1979; Winterer and Bosellini, 1981; Doglioni and Bosellini, 1987; Castellarin and Cantelli, 2000). Cretaceous to lower Eocene marine sediments crop out extensively in the Belluno Basin to the south

* Corresponding author. Department of Geosciences, University of Padova, Via Giotto 1, I-35137 Padova, Italy.
*E-mail address:* edoardo.dallanave@unipd.it (E. Dallanave).

0012-821X/$ – see front matter © 2009 Elsevier B.V. All rights reserved.
doi:10.1016/j.epsl.2009.05.033

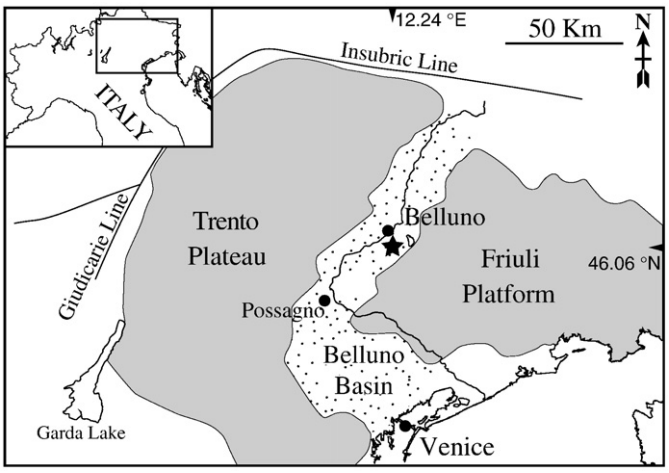


**Fig. 1.** Geologic sketch map of the Venetian Southern Alps with indication of key paleogeographic domains. The Cicogna section (star; Lat. = 46.06 °N; Long. = 12.24 °E) is located in the Belluno Basin ~8 km to the south of the town of Belluno along the Cicogna riverbed.

of the town of Belluno, where the Cicogna section of this study is located (Fig. 1). These pelagic to hemipelagic sediments, up to 200–250 m in thickness, are mainly represented by well bedded, pink to red limestones and marly limestones, hereafter referred to as Scaglia Rossa *sensu lato (s.l.)*, which includes lithostratigraphic units that still need formal ratification (Di Napoli Alliata et al., 1970; Costa et al., 1996). The Scaglia Rossa *s.l.* is overlain by lower–middle Eocene mainly siliciclastic turbidites pertaining to the Belluno Flysch (Stefani and Grandesso, 1991), which represents the foredeep deposits of the west-verging Dinaric thrusts (Doglioni and Bosellini, 1987).

### 2.1. The Cicogna section

The Cicogna section (46.06°N, 12.24°E) is located about 8 km south of Belluno along the Cicogna riverbed (Fig. 1), and consists of ~81 m of continuously exposed hemipelagic sediments pertaining to the Scaglia Rossa *s.l.*, capped by the Belluno Flysch (Fig. 2). Bedding planes dip to the NW (~315°N) by about ~45°. The basal 20 m of the section consists of gray-greenish couplets of marlstones and marly limestones, which are replaced, from ~20 m up to 28.7 m by pink-reddish marls with no apparent rhythmicity. The interval comprised between 28.7 m and 31.7 m consists of clayey marls attributed to the Clay Marl Unit (CMU), which represents the lithological expression of the PETM in the Belluno Basin (Giusberti et al., 2007). The interval from the top of the CMU up to 39.2 m is characterized by the re-occurrence of marl-limestone couplets, whereas from 39.2 m up to ~75.0 m at the first significant inception of siliciclastic material of the Belluno Flysch, the succession is essentially characterized by red marls with no apparent rhythmicity. Finally, the interval from 75.0 m to 80.6 m is characterized by red marls alternating with siliciclastic layers, which become dominant from 80.6 m (formal base of the Belluno Flysch) upward (Fig. 2).

## 3. Calcareous nannofossil biostratigraphy

Calcareous nannofossil analyses have been performed on 185 samples taken on average every 1 m; a sampling resolution of 10–20 cm was adopted close to key biohorizons and across critical intervals like the PETM. Standard smear-slides were prepared from all samples. The material was disaggregated by mechanical means and no anomalous or selective breakage due to preparation was observed. The nannofossil size fraction was not concentrated through settling techniques. Calcareous nannofossils were observed in the light microscope Zeiss Axiophot 40 at a magnification of 1250×. The taxonomy used in this paper is described in Perch-Nielsen (1985), and the zonal schemes adopted are those of Martini (NP; 1971) and Okada and Bukry (CP; 1980). Taxa abundances were determined by counting the index species along three smear-slide transects (representing an area of about 9 $mm^2$). The abundance patterns of *Fasciculithus*, *Zygrhablithus* and *Girgisia gammation* were determined by counting index species in a prefixed area (1 $mm^2$) (Backman and Shackleton, 1983). Abundance patterns of *Discoaster araneus*, *Discoaster anartios,* and *Sphenolithus radians* were determined by counting a prefixed number of taxonomically related forms (Rio et al., 1990), i.e., 50 discoasterids and 100 sphenoliths. The calcareous nannofossil biohorizons have been defined using the abundance patterns of the index species as follows: Lowest Occurrence (LO), Lowest Rare Occurrence (LRO), Lowest Common Occurrence (LCO), Highest Occurrence (HO), Highest Common Occurrence (HCO) and Crossover (CO) (see Raffi et al., 2006 for additional information).

Calcareous nannofossil assemblages are usually rich and well diversified, and the preservation varies from poor to moderate. Reworked forms are rare, saved for discrete, siliciclastic-rich intervals containing reworked Cretaceous specimens. In the lower part of the section, the assemblages are mainly composed of common *Toweius* and *Coccolithus* in association with *Sphenolithus*, *Fasciculithus*, *Zygrhablithus, Prinsius*, *Discoaster, Ericsonia*, and *Octolithus*. Upward, the relative abundance of heterococcoliths, which mainly consist of *Coccolithus* and *Toweius*, show a gradual decrease, associated with a prominent increase of *Sphenolithus* and *Zygrhablithus*.

In particular, we identified the following main calcareous nannofossil biohorizons (Fig. 2, Table A1).

- The LO of *Discoaster mohleri*, which defines the base of Zone NP7 (or CP6). In the Cicogna section, *D. mohleri* is found to be continuously present from the section base.
- The LO of *Discoaster multiradiatus*, which marks the base of Zone NP9a (and CP8a). This biohorizon occurs at the 9.90 m level and represents one of the most reliable Paleocene datums.
- The LO and HO of *Ericsonia robusta*, which designate a distinct stratigraphic range; in particular, the LO of *E. robusta*, observed at the 3.97 m level, shortly precedes the LO of *D. multiradiatus*, while the HO of *E. robusta*, identified at the 11.2 m level, correlates with the C25n/C24r boundary.
- Some heavily calcified *Fasciculithus* species suffered an abrupt extinction in correspondence with the onset of the PETM interval, which occurs at the 27.73 m level, thus decreasing the species diversity significantly.
- The LOs of the genus *Rhomboaster* and the Calcareous Nannofossil Excursion Taxa (CNET), which include *Rhomboaster calcitrapa* gr., *D. anartios,* and *D. araneus*, are used to subdivide Zones CP8 and NP9 (Bukry, 1973; Aubry et al., 2000). These unusual taxa are found to be stratigraphically restricted to the PETM, being distributed from 28.88 m to 32.52 m.
- *Fasciculithus* shows a first marked decrease in abundance in coincidence with the bloom of *Zygrhablithus bijugatus* at the 31.60 m level. The final extinction of this genus occurs above the PETM at the 34.73 m level.
- The *Tribrachiatus* lineage, which includes *T. bramlettei, T. contortus,* and *T. orthostylus*, provides several valuable biohorizons that are

**Fig. 2.** The late Paleocene–early Eocene Cicogna section. To the left: lithostratigraphic log of the section [T1 = Carbonate turbidite level; T2 = Sandy turbidite level; T3 = Belluno Flysch turbidite; CMU = clay marl unit (Giusberti et al., 2007); the carbonate content is referred to the Scaglia Rossa *s.l.* formation]. In the mid part of the diagram are the abundance patterns of selected calcareous nannofossil species discussed in the text. To the right are the standard nannofossil zonations placed next to magnetic polarity zones shown by filled (open) bars for normal (reverse) polarity, which have been correlated to the CK95 geomagnetic polarity time scale (Cande and Kent, 1995). See text for discussion.

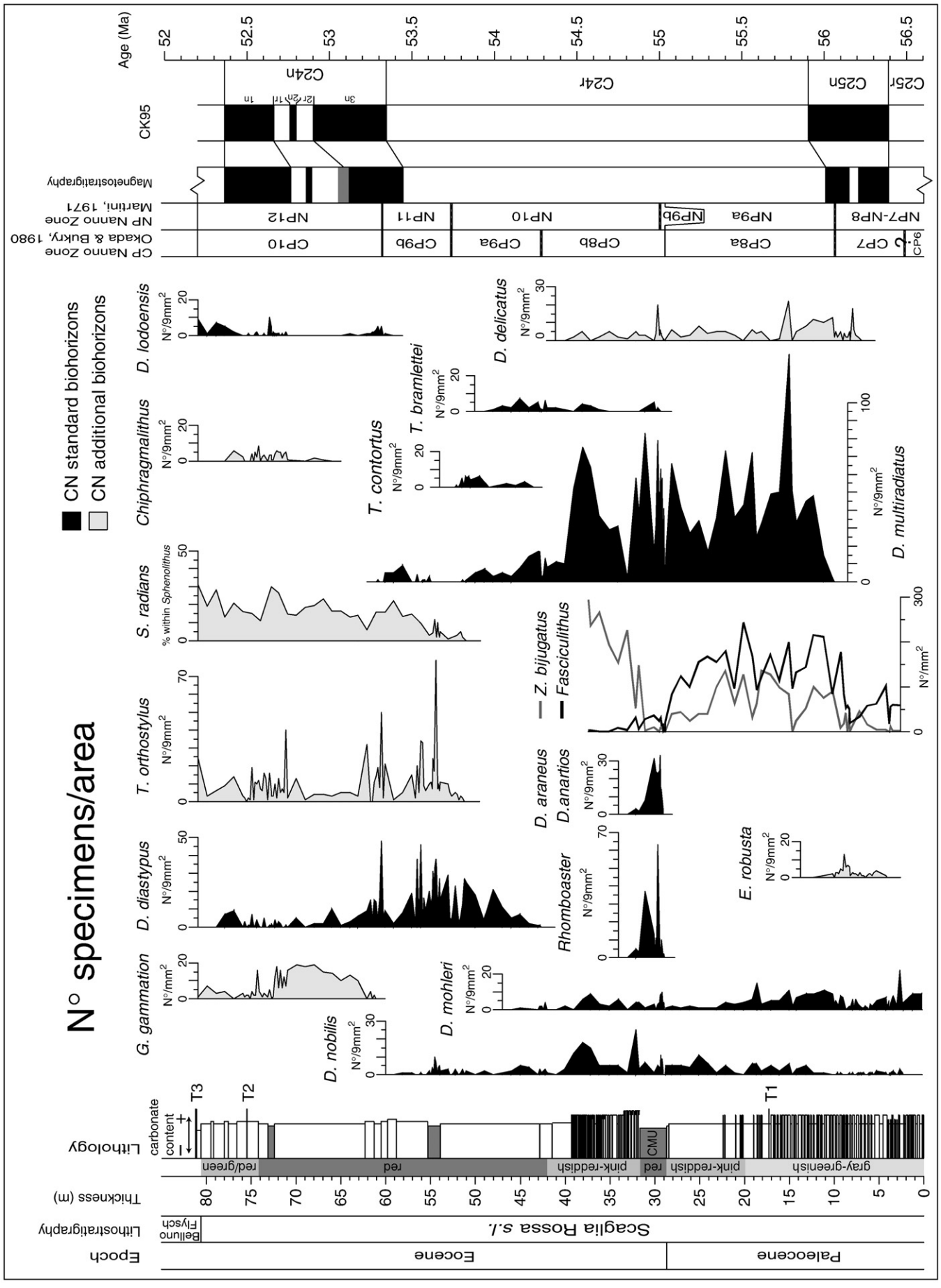
Age (Ma)
52
52.5
53
53.5
54
54.5
55
55.5
56
56.5
CK95
Magnetostratigraphy
C24n
C24r
C25n
C25r
3n
2r
2n
1r
1n
CP Nanno Zone
Okada & Bukry, 1980
NP Nanno Zone
Martini, 1971
CP10
CP9b
CP9a
CP8b
CP8a
CP7
CP6
NP12
NP11
NP10
NP9b
NP9a
NP7-NP8
Epoch
Lithostratigraphy
Thickness (m)
Lithology
carbonate content
Bellino Flysch
Scaglia Rossa s.l.
Eocene
Paleocene
gray-greenish
pink-reddish
red
CMU
red/green
T1
T2
T3
N° specimens/area
CN standard biohorizons
CN additional biohorizons
D. lodoensis
Chiphragmalithus
S. radians
% within Sphenolithus
T. orthostylus
D. diastypus
G. gammation
D. nobilis
D. mohleri
T. contortus
T. bramlettei
D. delicatus
D. multiradiatus
Z. bijugatus
Fasciculithus
D. araneus
D.anartios
Rhomboaster
E. robusta
N°/9mm2
N°/mm2

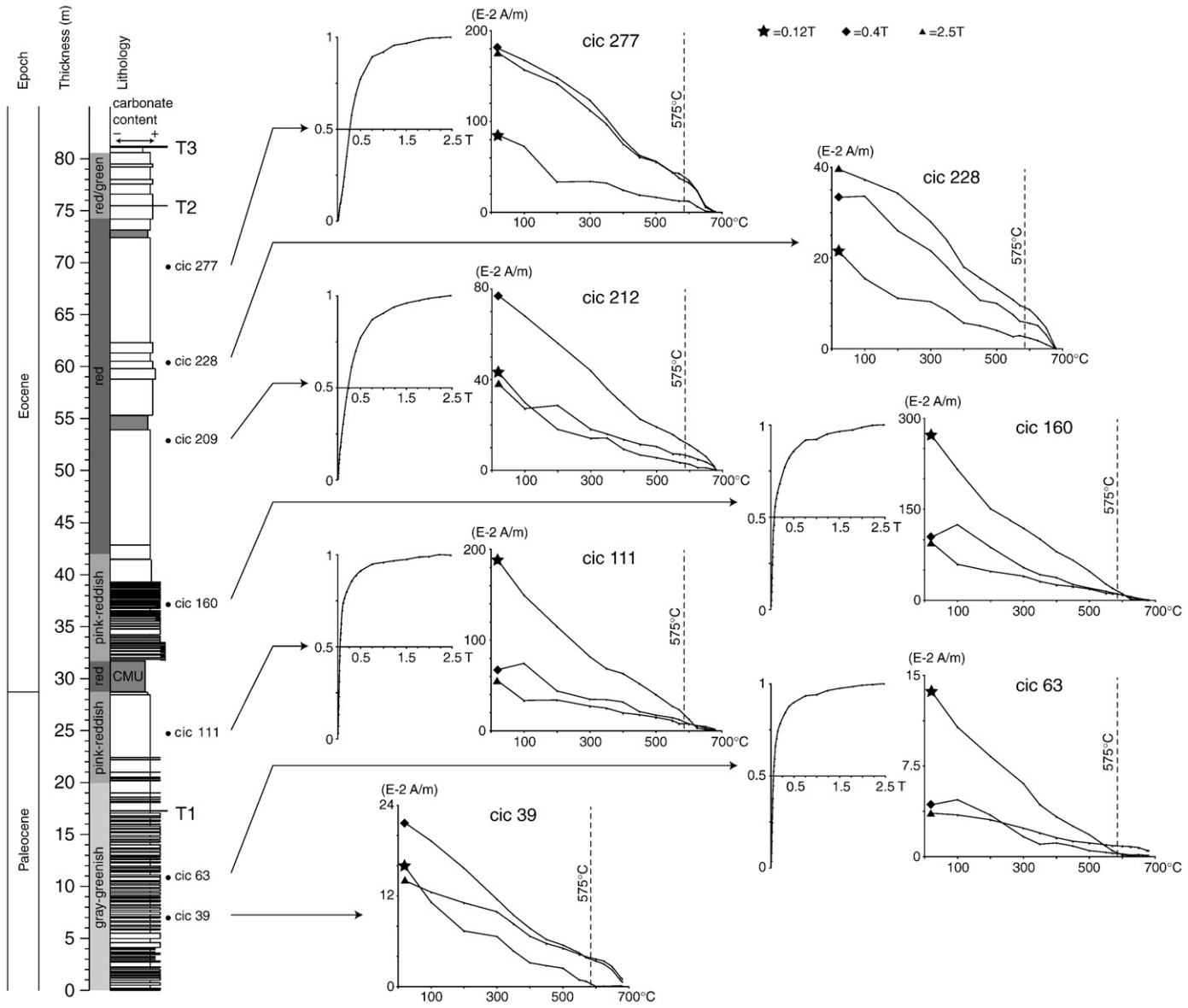


**Fig. 3.** Isothermal Remanent Magnetization (IRM) acquisition curves (normalized) and thermal unblocking characteristics of orthogonal axis IRMs for representative samples of the Cicogna section.

used to subdivide the early Eocene. The LO of *T. bramlettei*, at the 29.43 m level, marks the base of Zone NP10; the LO of *T. contortus*, at the 45.50 m level, defines, together with the LO of *Discoaster diastypus* (at the 42.70 m level), the base of Zone CP9a (Bukry, 1973); the HO of *T. contortus*, at the 52.70 m level, identifies the base of Zone NP11 (or CP9b). In addition, the extinction of *T. contortus* well correlates with three additional bioevents, namely the LOs of *T. orthostylus* and *S. radians*, found at the 51.30 m level, and the HCO of *D. multiradiatus*, observed at the 51.50 m level.

- The LO of *D. lodoensis* at the 60.40 m level is followed by an absence interval up to 71.10 m, from which level *D. lodoensis* has been consistently found again (*D. lodoensis* LCO). The LCO of *D. lodoensis* has been found to virtually coincide with the LCO of circular *Chiphragmalithus* (albeit circular specimens ascribable to this genus have been sporadically observed from the 66.5 m level).
- The LO of *G. gammation* lies between the LO and LCO of *D. lodoensis* at the 61.20 m level. This biohorizon is potentially useful to subdivide Zone CP9b (or NP11).

These biostratigraphic events indicate that the Cicogna section appears to be stratigraphically complete at least to within nannofossil biostratigraphic resolution, and spans a late Paleocene–early Eocene time interval encompassing Zones NP7/NP8–NP12, equivalent to Zones CP6–CP10. The Paleocene–Eocene boundary is placed at the base of the Clay Marl Unit and virtually coincides with the LOs of the genus *Rhomboaster* and the Calcareous Nannofossil Excursion Taxa, which define the base of Zones CP8b and NP9b (Bukry, 1973; Aubry et al., 2000).

## 4. Paleomagnetism

Paleomagnetic samples were drilled and oriented in the field at an average sampling interval of ~0.25 m giving a total of 319 standard ~11 cc specimens for analyses, conducted at the Alpine Laboratory of Paleomagnetism (Cuneo, Italy). A representative suite of samples was subjected to rock magnetic analysis using isothermal remanent magnetization (IRM) acquisition curves up to 2.5 T imparted by an *ASC Pulse Magnetizer*. The IRM curves can be divided into two groups,

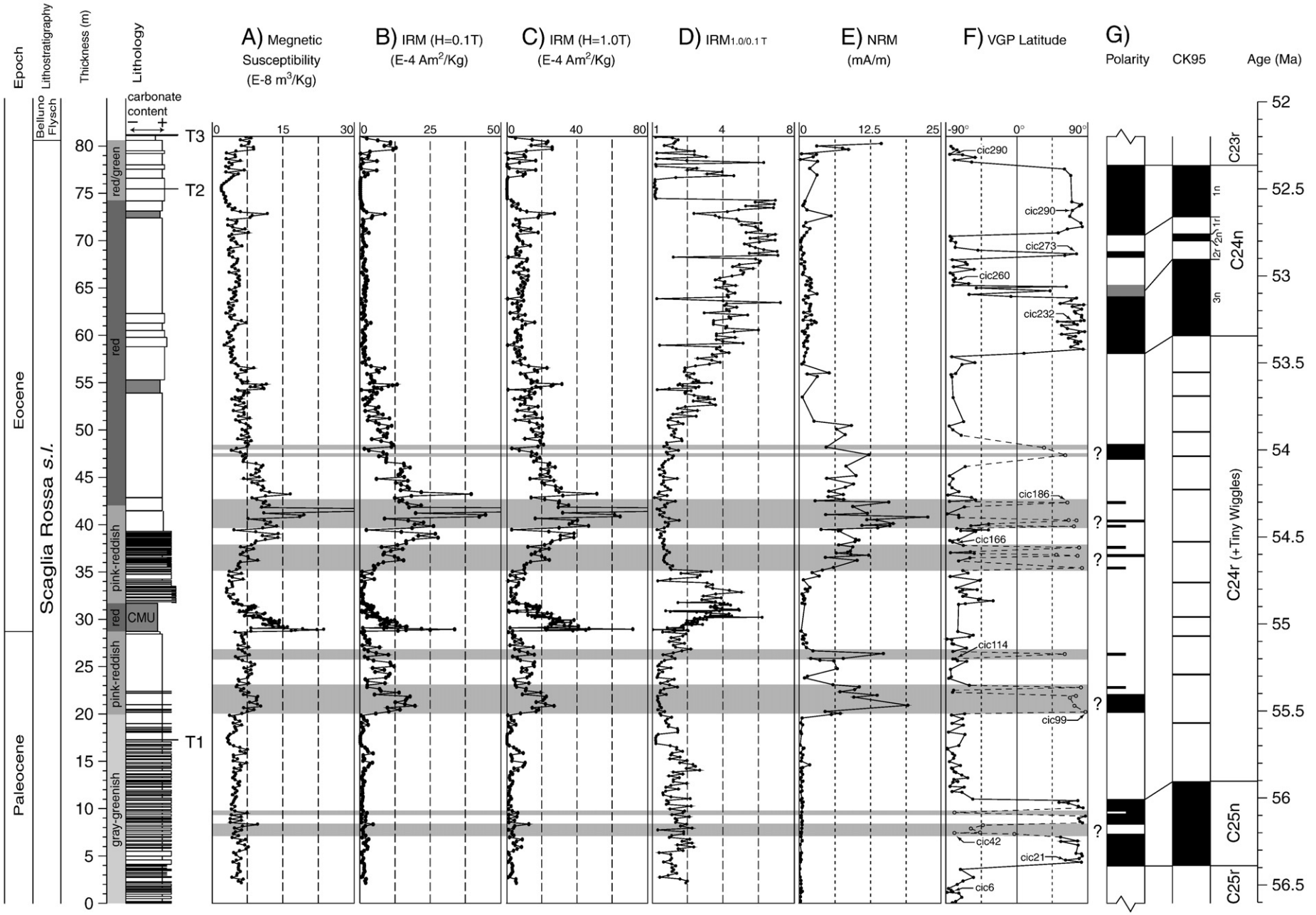


**Fig. 4.** Magnetic stratigraphy of the Cicogna section. Columns A–E summarize the main magnetic properties of the section as discussed in the text; column F reports the latitude of the virtual geomagnetic poles used to erect the magnetic polarity stratigraphy (G; black for normal polarity, white for reverse polarity); the correlation with the CK95 geomagnetic polarity time scale of Cande and Kent (1995) is also indicated. See text for discussion.

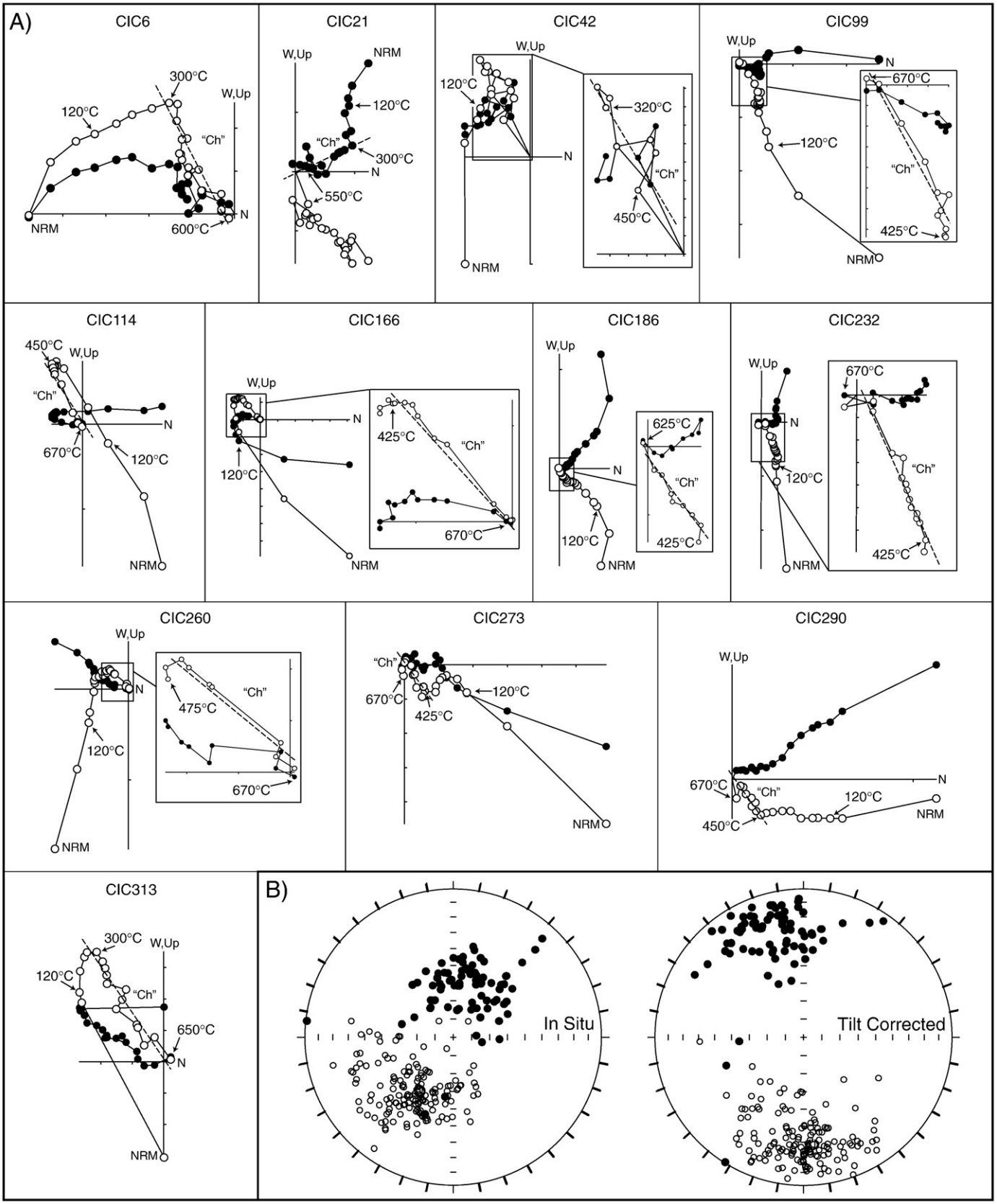


**Fig. 5.** (A) Vector end-point demagnetization diagrams of NRM of representative samples from the Cicogna section. Closed circles are projections onto the horizontal plane and open circles are projections onto the vertical plane in *in situ* coordinates. (B) Equal area projections before (*in situ*) and after bedding tilt correction for the characteristic "Ch" component directions from the Cicogna section. See text for discussion.

showing different behaviors. In samples collected from the lower gray-greenish to pink ~25 m of the section, the IRM increases initially steeply up to applied fields of ~0.2–0.3 T and then starts climbing gently without reaching saturation up to 2.5 T (Fig. 3, samples cic63, cic111). In samples collected from ~25 m up to the section top, the IRM increases initially less steeply up to fields of ~0.5 T and then continues to climb gently without reaching saturation up 2.5 T (Fig. 3, samples cic160, cic212, cic277). These types of behavior suggest the presence of variable amounts of low coercivity and high coercivity components, with a tendency for the high/low coercivity component ratio to increase upsection. These samples were successively subjected to thermal demagnetization of a three-component IRM imparted in 2.5, 0.4, and 0.12 T fields along three orthogonal directions (Lowrie, 1990) (Fig. 3). Thermal unblocking characteristics of orthogonal IRMs show that samples from the lower ~20 m of the section, green-gray in color, contain a low coercivity component (revealed by the 0.12 T curve) with maximum unblocking temperatures of ~570 °C interpreted as magnetite. The mid-high coercivity (0.4 T and 2.5 T) curves show maximum unblocking temperatures of 650–680 °C consistent with the occurrence of hematite; the presence in these curves of an inflection between ~300 and 400 °C suggests that at least part of this hematite may derive from the transformation of an original maghemite phase during thermal demagnetization treatment (Fig. 3, samples cic39 and cic63). From ~20 m up to the section top, where sediment color becomes progressively more red, samples show the exclusive presence of coercivity components with maximum unblocking temperatures around 650–680 °C, interpreted as hematite; similarly to what described above, the presence in the mid-high coercivity curves of an inflection between ~300 and 400 °C suggests the break-down of an original maghemite phase during thermal demagnetization (Fig. 3, samples cic111–cic277).

A total of 450 unoriented ~5 gr samples were also collected every 20 cm (every 5 cm across the CMU) to obtain detailed information on the rock-magnetic variations throughout the section. Magnetic susceptibility of each sample was measured on a AGICO KLY-3 Kappabridge susceptibility bridge (Fig. 4A). The samples were successively magnetized in 0.1 T and 1.0 T fields, and the values of the IRMs were measured on a *2G DC-SQUID* cryogenic magnetometer (Fig. 4B, C). The susceptibility and IRM curves show relatively high values corresponding to stratigraphic levels pertaining to the CMU as well as levels straddling the ~20–22 m and ~40–45 m interval. The 1.0/0.1 T IRM ratio ($IRM_{1.0/0.1\ T}$) (Fig. 4D) shows low values in the lower ~25 m of the section, followed by a ~7 m-thick excursion high values starting at the base of the CMU and ending above it at ~36 m. Above this level, the ratio follows a more progressive increasing trend from ~45 m up to the section top, interrupted by occasional levels with very low values correlative with more siliciclastic intervals. Recalling that the bulk rock-magnetic experiments showed that a magnetite–maghemite mixture dominates the lower gray-greenish ~20 m of the section, and that a hematite–maghemite mixture dominates the mid-upper part of the section, we conclude that the IRM ratio is ultimately controlled by the relative proportion of higher versus lower coercivity phases within the triad magnetite–maghemite–hematite, whereby the lower the ratio, e.g. in the lower ~20 m of the section, the higher the magnetite content, whereas the higher the ratio, e.g. across the CMU and from ~45 m upwards, the higher the contribution of hematite–maghemite.

The natural remanent magnetization (NRM) intensity of the 319 oriented ~11 cc specimens ranges between 0.04 and 22.6 mA/m with two peak values at ~20–27 and ~35–54 m that broadly correspond to those observed in the 0.1 and 1.0 T IRM curves (Fig. 4E). All the samples were demagnetized in maximum steps of 50 °C, and the component structure of the NRM was monitored after each demagnetization step by means of vector end-point demagnetization diagrams (Zijderveld, 1967); steps of 10–25 °C were adopted close to critical unblocking temperatures. Magnetic components were calculated by standard least-square analysis (Kirschvink, 1980) on linear portions of the demagnetization paths and plotted on equal-area projections.

Scattered magnetic component directions with positive (down-pointing) inclinations in geographic (*in situ*) coordinates have been commonly observed from room temperature up to an average of ~200–300 °C. Removal of these spurious magnetizations revealed the presence of a characteristic component linearly trending to the origin of the demagnetization axes. This characteristic component was isolated in 229 (71.5%) specimens by linear interpolation of the demagnetization steps from ~300 °C to ~525 °C in specimens from the lower ~20 m of the section (Fig. 5A, cic6–cic42), and from ~425 °C to ~625 °C in specimens from meter level ~20 to the section top (Fig. 5A, cic99–cic313). These characteristic magnetizations are oriented NE-and-down or SW-and-up in geographic (*in situ*) coordinates; after correction for homoclinal bedding tilt, they turn to NNW-and-down or SSE-and-up (Fig. 5B, Table 1). These populations depart from antipodality by ~16°, which we attribute to residual contamination from lower temperature components, and fail to pass the reversal test at the 95% level of confidence using the procedure suggested by Watson (1983) ($V_0 = 47.7$; $V_{critical} = 6.2$; for further details on the procedure, see also McFadden and McElhinny, 1990). The effect of the contaminating bias on the mean direction could be minimized by inverting all directions to common polarity, which resulted in a tilt corrected mean direction of Dec. = 355.4°, Inc. = 28.3° ($k = 12.2$, $\alpha_{95} = 2.8°$; Table 1).

To constrain the age of the characteristic magnetization and assign polarity to the NNW-and-down or SSE-and-up characteristic

**Table 1**
Characteristic component directions and paleomagnetic pole from the Cicogna section.

| N | MAD | Geographic (in situ) coordinates | | | | Bedding (tilt-corrected) coordinates | | | | |
|---|---|---|---|---|---|---|---|---|---|---|
| | | k | $\alpha_{95}$ | GDEC | GINC | k | $\alpha_{95}$ | BDEC | BINC | BINC* |
| Normal polarity directions | | | | | | | | | | |
| 79 | 7.7 ± 4.4 | 13.7 | 4.5 | 16.5 | 61.2 | 13.6 | 4.5 | 343.5 | 26.1 | – |
| Reverse polarity directions | | | | | | | | | | |
| 150 | 6.9 ± 3.9 | 13.7 | 3.2 | 218.5 | −50.8 | 13.6 | 3.2 | 181.8 | −29.1 | – |
| Reverse and normal polarity directions | | | | | | | | | | |
| 229 | 7.2 ± 4.1 | 12.4 | 2.8 | 32.2 | 54.8 | 12.2 | 2.8 | 355.4 | 28.3 | $53.1^{59.8}_{44.3}$ |

| Paleomagnetic pole Ci1 | | | | | Paleomagnetic pole Ci2 | |
|---|---|---|---|---|---|---|
| N | K | $A_{95}$ | LONG | LAT | LONG | LAT |
| 229 | 12.6 | 2.7 | 200.8 | 58.8 | 209.7 | 77.1 |

*N*=number of sample; MAD=mean angular deviation of the mean paleomagnetic direction expressed in degrees; *k* and K=Fisher precision parameter of the mean paleomagnetic direction and pole, respectively; $\alpha_{95}$ and $A_{95}$=Fisher angle of half cone of 95% confidence about the mean paleomagnetic direction and pole, respectively; GDEC and GINC=declination and inclination in geographic (*in situ*) coordinates of the mean paleomagnetic direction; BDEC and BINC=declination and inclination in bedding (tilt-corrected) coordinates of the mean paleomagnetic direction; BINC*=inclination of the mean paleomagnetic direction corrected for inclination shallowing; LONG and LAT=longitude and latitude of the mean paleomagnetic pole before (Ci1) and after (Ci2) correction for inclination shallowing.

directions, we compared the mean paleomagnetic pole from Cicogna (Ci1; Long. = 200.8°E, Lat. = 58.8°N, $A_{95}$ = 2.7°; Fig. 6A, Table 1), obtained by averanging the virtual geomagnetic poles (VGPs) of the characteristic component directions, to the late Cretaceous–early Miocene master apparent polar wander (APW) path for Africa of Besse and Courtillot (2002, 2003). The paleogeographic affinity of the Southern Alps with Africa has been demonstrated at least since the Permian (Muttoni et al., 2001) insofar as relatively less deformed regions of Adria such as the Adriatic foreland or portions of the Southalpine chain (e.g., the Dolomites) maintained substantial tectonic coherence (within paleomagnetic resolution) with Africa during Alpine deformation in the Cenozoic (Muttoni et al., 2003; Muttoni et al., 2004; Rosenbaum et al., 2004; Agnini et al., 2006). The Cicogna Ci1 paleopole is however removed from the late Paleocene–

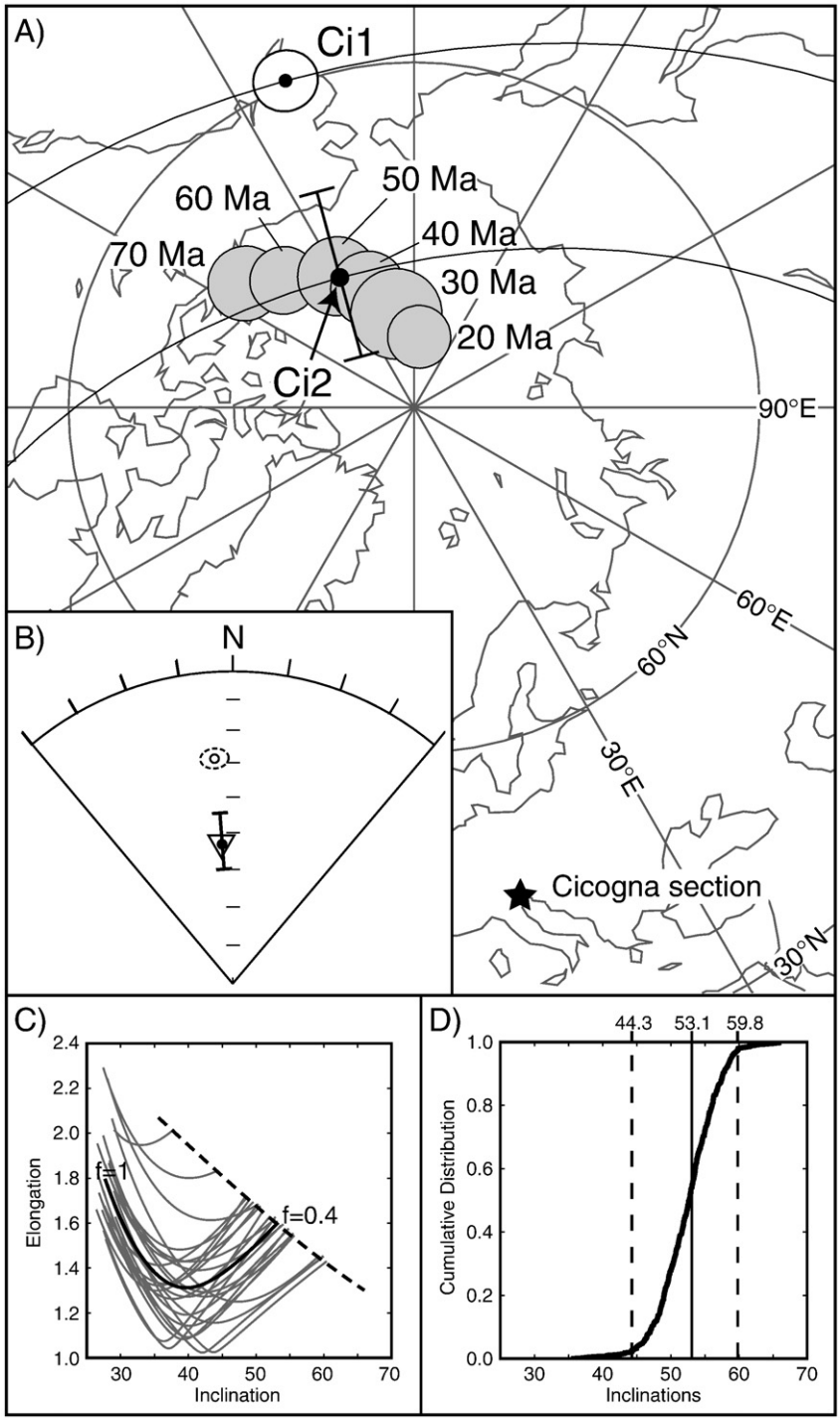


**Fig. 6.** (A) The mean paleomagnetic pole from the Cicogna section before (Ci1) and after (Ci2) directional unflattening is compared to the master apparent polar wander path of Africa for the 20–70 Ma interval (Besse and Courtillot, 2002, 2003) (map drown with PaleoMac; Cogné, 2003). (B) The characteristic mean direction from the Cicogna section before (open circle) and after (closed circle) directional unflattening, with the associated 95% confidence boundaries (dashed circle and error bar, respectively); these mean directions are compared to the mean direction expected at Cicogna from the 50 Ma paleopole of Africa (open triangle). (C) The *E*/*I* values of the systematically unflattened directions with the unflattening parameter *f* ranging from 1 to 0.4 (heavy line) are compared to the E/I values predicted by the TK03.GAD geomagnetic field model (dashed line). 25 of 500 boostrapped dataset are shown by the light lines. (D) Diagram of the cumulative distribution of all inclinations derived from the bootstrapped crossing points, with the associated 95% confidence boundaries (44.3°–59.8°) around the mode (53.1°).

early Eocene APW path of Africa by ~18° in the far-side direction of the sampling site (Fig. 6A). This is because the characteristic component mean direction is shallower by ~25° with respect to the inclination expected at Cicogna from the African APW path (Fig. 6B). The mean unblocking temperature of characteristic component and the rock-magnetic analyses suggest that the magnetization at Cicogna is carried primarily by hematite. Hematite particles can be associated with magnetic inclination that is shallower compared to the external geomagnetic field direction (Tauxe and Kent, 1984). We used the elongation/inclination ($E/I$) method of Tauxe et al. (2008) to detect and correct for inclination shallowing. In brief, a given directional data set is progressively "unflattened" and the elongation parameter $E$ is evaluated at each unflattening step with the aim to find the unflattening level ($f$) at which the inclination and elongation are consistent with a statistical dipole field model (TK03.GAD; see Tauxe et al., 2008 for further information).

We systematically unflattened the Cicogna characteristic directions by applying values of $f$ ranging from 1 to 0.4, and at each unflattening step, $E/I$ values were calculated (Fig. 6C, heavy curve); at $f=0.4$, the $E/I$ pair most consistent with the TK03.GAD field model (Fig. 6C, dashed line) was attained. To assess the uncertainty of this estimate, we repeated the analysis by means of bootstrap technique;

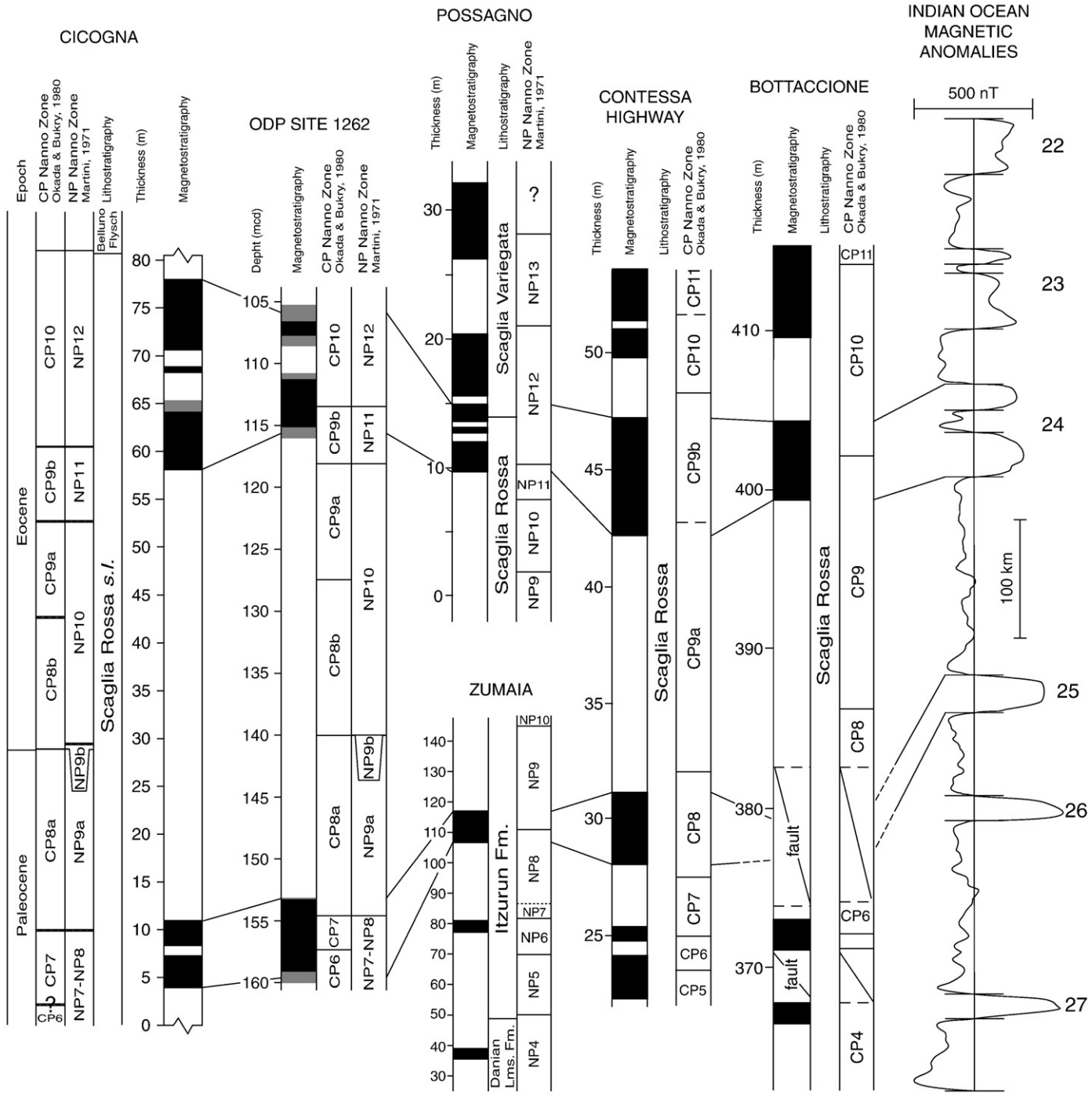


**Fig. 7.** The magneto-biostratigraphy of the Cicogna section is correlated to coeval magneto-biostratigraphies from ODP Site 1262, Possagno (Venetian Southern Alps, Italy), Zumaia (Basque Basin, Spain), Contessa Highway and Bottaccione (Central Apennines, Italy), as well as to a composite stacked profile of Indian Ocean marine magnetic anomalies from anomaly 27 to 22 (Cande and Kent, 1992). See text for discussion.

25 of 500 examples of bootstrapped data are shown as light lines in Fig. 6C. The corrected (unflattened) mean charcteristic inclination and associated 95% confidence band (Inc. = $53.1^{59.8}_{44.3}$, Fig. 6D) is now in excellent agreement with the inclination expected at Cicogna from the 50 Ma paleopole of Africa (Fig. 6B). The Cicogna paleopole position after the shallow bias correction (Ci2; Long. = 209.7°E, Lat. = 77.1°N; Table 1) is virtually indistinguishable from the 50 Ma African paleopole (Fig. 6A). We can therefore consider this part of the Alps as tectonically coherent with Africa since the late Paleocene.

## 5. Magnetostratigraphy

For each sample characteristic magnetization, a virtual geomagnetic pole (VGP) was calculated. The latitude of the samples VGP relative to the mean paleomagnetic (north) pole axis was used for interpreting polarity stratigraphy (Lowrie and Alvarez, 1977; Kent et al., 1995). VGP relative latitudes approaching +90°N or −90°S are interpreted as recording normal or reverse polarity, respectively (Fig. 4F). The VGP data show a ~4 m-thick reverse polarity interval at the base of the section, followed by ~7 m of dominantly normal polarity embedding a ~1 m thick reverse polarity interval documented by five samples (Fig. 4F, G). A reverse polarity sample at 9.6 m was also found. From ~11 m to ~57.7 m, the VGP curve shows prevalent reverse polarity, interrupted by several short normal polarity events in the ~20–49 m interval. These events are mainly represented by one or two specimens, except for the ~2 m-thick interval centered at ~21 m with 4 consecutive normal polarity specimens; these events seem to show a consistent correlation to peak values of susceptibility, IRM, and NRM (Fig. 4). Finally, from ~57.7 m up to the section top (~81 m), the VGP curve shows a well-defined sequence of normal and reverse polarity intervals (Fig. 4F, G).

We compared the Cicogna magneto-biostratigraphy to coeval data from classic sections from the literature, namely Possano from the Southern Alps (Agnini et al., 2006), Bottaccione and Contessa Highway from the Northern Appennines near Gubbio (Lowrie et al., 1982; Napoleone et al., 1983; Monechi and Thierstein, 1985), as well as Zumaia from the Basque Basin (Dinarès-Turell et al., 2002, 2003, 2007) and ODP Site 1262 from the Walvis Ridge (Agnini et al., 2007 and

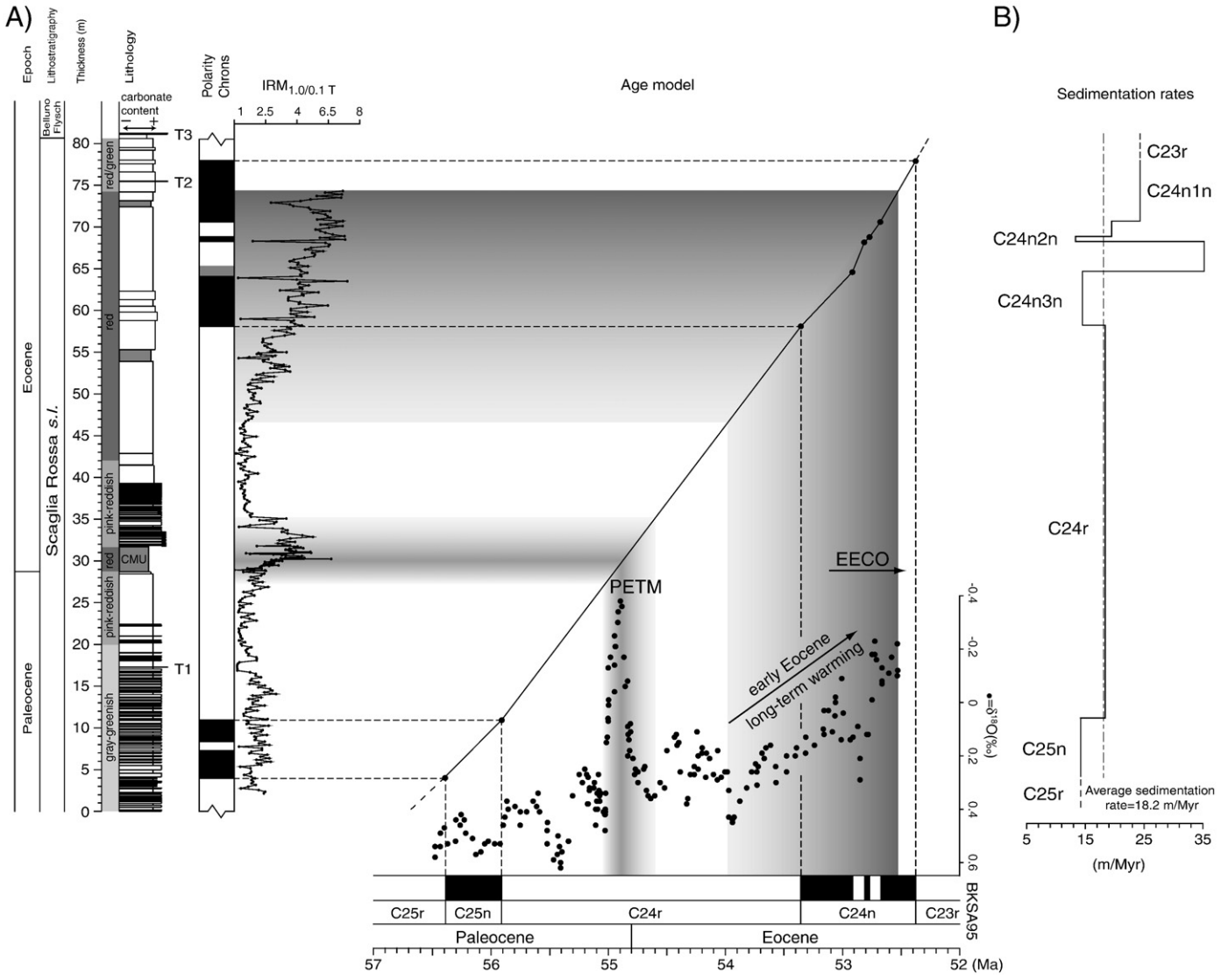


**Fig. 8.** Age-depth model and derived sediment accumulation rates for the Cicogna section obtained by magnetostratigraphic correlation to the CK95 geomagnetic polarity time scale of Cande and Kent (1995). $IRM_{1.0/0.1\ T}$ values are plotted on the vertical axis to show the correlation with the $\delta^{18}O$ dataset of Miller et al. (2005; horizontal axis). The gray bands highlight positive correlations between high $IRM_{1.0/0.1\ T}$ values (corresponding to high amounts of maghemite–hematite) and low $\delta^{18}O$ values, indicative of warm climate e.g., during the PETM. See text for discussion.

reference herein) (Fig. 7). An excellent magnetostratigraphic matching straddling similar nannofossil zonations was observed between the Cicogna section and the correlative sections from the literature. All these sections could be correlated to the stacked profile of magnetic anomalies 22–27 from the Indian Ocean (Cande and Kent, 1992) (Fig. 7). Within this correlation framework, we observe that the frequently single sample-based normal polarity events present at Cicogna in the ~20–49 m interval and that correlate to peak values of rock-magnetic parameters (Fig. 4), have no obvious counterparts in any of the coeval sections discussed above, nor can be successfully correlated to known tiny wiggles present between marine magnetic anomaly 25 and 24 (Figs. 4G and 7; Cande and Kent, 1992). Hence, we interpret the northward-and-down characteristic directions isolated in these samples as overprints of diagenetic origin recording a post-depositional geomagnetic field of normal polarity. In addition, the ~1 m-thick reverse polarity interval found at Cicogna within Chron C25n (Figs. 4G and 7) was not observed elsewhere in seemingly correlative levels (Fig. 7), and is therefore provisionally considered as dubious. On the basis of these considerations, the Cicogna section shows an overall sequence of 9 magnetozones, encompassing marine magnetic anomalies from 25 to 23 and Chrons from C25r to C23r.

## 6. Age model of sedimentation and biochronology

We constructed an age-depth plot and derived sediment accumulation rates at Cicogna by means of magnetostratigraphic correlation to the geomagnetic polarity time scale of Cande and Kent (1995; CK95) across the C25r–C23r interval, assuming constant sedimentation rate between magnetochronologic control points (Fig. 8A). We adopted a total of 8 magnetic polarity reversals as chronologic control points, identified between the base of Chron C25n and the top of Chron C24n. The derived age model implies a relatively constant average sediment accumulation rate of ~18 m/Myr throughout the section (Fig. 8B).

Our CK95-based age-depth function has been used to place the sequence of biohorizons recognized at Cicogna in a temporal reference frame for comparison with similar bioevents reported in the BKSA95 time scale, as well as with recent data from ODP Site 1262. Our age-depth function has been also used to place the rock-magnetic variability previously described, particularly the $IRM_{1.0/0.1\ T}$ ratio, in a same temporal reference frame for comparison with climate-proxy data from the literature, as discussed below.

## 7. Discussion and conclusions

Apart from standard biohorizons, whose ranking and spacing have found to be largely consistent with previous studies (e.g., Backman, 1986; Berggren et al., 1995; Raffi et al., 2005; Agnini et al., 2007 and references herein), the Cicogna section provides several new bioevents in the NP9–NP10 (CP8–CP9a) interval within Chron C24r that were not previously recognized (hence included) in the BKSA95 reference time scale; several of these new biohorizons have been

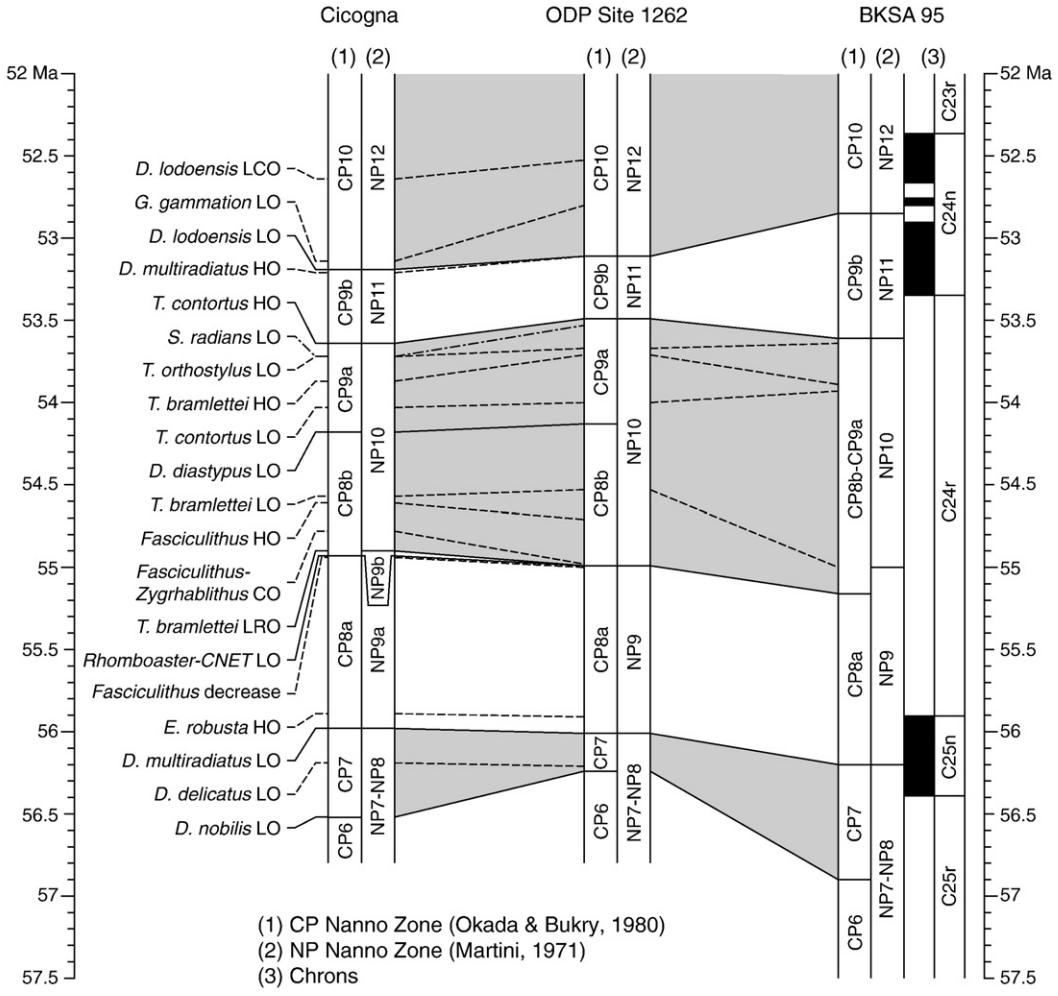


**Fig. 9.** Biochronologic correlation between the Cicogna section, ODP Site 1262, and the BKSA95 time scale (Berggren et al., 1995); see text for details.

recently observed also at ODP Site 1262 (Fig. 9; Table A1). In particular, useful bioevents were found in the mid part of Chron C24r across the P–E boundary, calibrated to ~54.94 Ma according to our age model; these include:

- The decrease in diversity of the genus *Fasciculithus* at ~54.93 Ma.
- The LOs of the Calcareous Nannofossils Excursion Taxa at ~54.94 Ma, virtually coinciding with the base of Zone CP8b, used to approximate the P–E boundary.
- The crossover in abundance between *Fasciculithus* and *Z. bijugatus* at ~54.8 Ma.
- The HO of the *Fascichulitus* at ~54.6 Ma.

These bioevents are constrained to a very short time interval and are likely related to environmental perturbations associated with the PETM (e.g., Gibbs et al., 2006, Agnini et al., 2007). Above the PETM, three additional bioevents have been identified in the upper part of Chron C24r at ~53.7 Ma (Zone NP11), namely the LO of *S. radians*, the LO of *Tribrachiatus orthostylus*, and the HCO of *D. multiradiatus*. Finally, useful bioevents have been also found within Chron C24n, namely the HO of *D. multiradiatus* at ~53.21 Ma, the LO of *G. gammation* at ~53.1 Ma, and the LO and LCO of *D. lodoensis* at ~53.19 Ma and ~52.6 Ma, respectively (Fig. 9; Table A1).

These new magneto-biostratigraphic data from the expanded and continuously exposed Cicogna section represent an improvement of the late Paleocene–early Eocene chronology, which is not well defined in current time scales (e.g., BKSA95) essentially because of the presence of unconformities in several deep-sea and shallow water sections from the literature (Aubry et al., 1996) and the substantial lack of reference sections provided with a complete and expanded Chron C24r interval (Fig. 7).

In regards to the rock-magnetic properties of the sediments, we observed high $IRM_{1.0/0.1\ T}$ values interpreted as due to high relative amounts of hematite–maghemite in levels attributed to the PETM as well as in levels dated from ~54 Ma to ~52.5 Ma (Fig. 8A). These variations are likely primary in origin; in fact, the Cicogna sediments contain a magnetic remanence carried by hematite and affected by inclination shallowing, which is typical for detrital (i.e., primary) hematite, albeit secondary hematite, possibly associated with normal polarity overprinting, has been also recognized in discrete levels within Chron C24r (Fig. 4, gray bands). We speculate that this (largely) primary rock-magnetic variability may be associated with (global) climate variability. In particular, warm and humid climate conditions typical of the PETM and the early Eocene (e.g., Wolfe, 1980; Estes and Hutchison, 1980; Axelrod, 1984; Zachos et al., 2001), characterized by enhanced continental weathering and runoff (e.g., Sloan and Rea, 1995), may have promoted the formation (and consequent transport and accumulation) of oxidized mineral phases such as maghemite and hematite (e.g., Singer et al., 1996; Barron and Torrent, 2002; Wilson, 2004). In this respect, high relative amounts of detrital hematite–maghemite in the ~55–54.5 Ma interval across the PETM, as well as from ~54 Ma to ~52.5 Ma, seem to correlate to warm global climate conditions as revealed by the benthic $\delta^{18}O$ climate-proxy record of Miller et al. (2005) (Fig. 8A). Several mechanisms able to explain (or reject) this apparent coupling between rock-magnetic variability and global climate, including the weathering of silicate rocks as a buffer to long-term climate change as first described by Walker and Hays (1981), are presently under scrutiny by the authors and will be discussed in a parallel paper.

## Acknowledgements

We thank Lisa Tauxe, Dennis V. Kent, and two anonymous reviewers for useful comments that improved this manuscript. E. Dallanave, C. Agnini and D. Rio were supported by MIUR-PRIN Grant # 2007W9B2WE_004.

## Appendix A. Supplementary data

Supplementary data associated with this article can be found, in the online version, at doi:10.1016/j.epsl.2009.05.033.

## References

Agnini, C., Muttoni, G., Kent, D.V., Rio, D., 2006. Eocene biostratigraphy and magnetic stratigraphy from Possagno, Italy: the calcareous nannofossils response to climate variability. Earth Planet. Sci. Lett. 241, 815–830.

Agnini, C., Fornaciari, E., Raffi, I., Rio, D., Röhl, U., Westerhold, T., 2007. High-resolution nannofossil biochronology of middle Paleocene to early Eocene at ODP Site 1262: implications for calcareous nannoplankton evolution. Mar. Micropaleontol. 64, 215–248.

Aubry, M.-P., Berggren, W.A., Stott, L., Sinha, A., 1996. The upper Paleocene–lower Eocene stratigraphic record and the Paleocene–Eocene boundary carbon isotopes excursion: implications for geochronology. Special Publications, vol. 101. Geological Society, London, pp. 353–380. doi:10.1144/GSL.SP.1996.101.01.18.

Aubry, M.-P., Cramer, B.S., Miller, K.G., Wright, J.D., Kent, D.V., Olsson, R.K., 2000. Late Paleocene event chronology: unconformities, not diachrony. Bull. Soc. Géol. Fr. 171 (3), 367–378.

Axelrod, D.I., 1984. An interpretation of Cretaceous and Tertiary biota in polar regions. Palaeogeogr. Palaeoclimatol. Palaeoecol. 45, 105–147.

Backman, J., 1986. Late Paleocene to Middle Eocene calcareous nannofossil biochronology from the Shatsky Rise, Walvis Ridge and Italy. Palaeogeogr. Palaeoclimatol. Palaeoecol. 57, 43–59.

Backman, J., Shackleton, N.J., 1983. Quantitative biochronology of Pliocene and early Pleistocene calcareous nannoplankton from theAtlantic, Indian and PacificOceans. Mar. Micropaleontol. 8, 141–170.

Barron, V., Torrent, J., 2002. Evidence for a simple pathway to maghemite in Earth and Mars soils. Geochim. Cosmochim. Acta 66, 2801–2806.

Berggren, W.A., Kent, D.V., Swisher III, C.C., Aubry, M.-P., 1995. A revised Cenozoic geochronology and chronostratigraphy. In: Berggren, W.A., et al. (Ed.), Geochronology, Time Scales and Global Stratigraphy Correlation. In: Spec. Publ., vol. 54. Soc. for Sediment. Geol., Tulsa, Okla, pp. 129–212.

Besse, J., Courtillot, V., 2002. Apparent and true polar wander and the geometry of the geomagnetic field over the last 200 Myr. J. Geophys. Res. 107 (B11), 2300. doi:10.1029/2000JB000050.

Besse, J., Courtillot, V., 2003. Correction to "Apparent and true polar wander and the geometry of the geomagnetic field over the last 200 Myr". J. Geophys. Res. 108 (B10), 2469. doi:10.1029/2003JB002684.

Bukry, D., 1973. Low-latitude coccolith biotratigraphic zonation. Proc. Ocean Drill. Prog. Sci. Results 15, 685–703.

Cande, S.C., Kent, D.V., 1992. A new geomagnetic polarity time scale for the Late Cretaceous and Cenozoic. J. Geophys. Res. 97, 13917–13951.

Cande, S.C., Kent, D.V., 1995. Revised calibration of the geomagnetic polarity time scale for the Late Cretaceous and Cenozoic. J. Geophys. Res. 100 (B4), 6093–6096. doi:10.1029/94JB03098.

Castellarin, A., Cantelli, L., 2000. Neo-Alpine evolution of the Southern Eastern Alps. J. Geodyn. 30, 251–274.

Cogné, J.P., 2003. PaleoMac: a Macintosh™ application for treating paleomagnetic data and making plate reconstructions. Geochem. Geophys. Geosyst. 4 (1), 1007. doi:10.1029/2001GC000227.

Costa, V., Doglioni, C., Grandesso, P., Masetti, D., Pellegrini, G.B., Tracanella, E., 1996. Carta Geologica d'Italia, Foglio 063, Belluno. Roma, Servizio Geologico d'Italia, scale 1:50,000, 1 sheet + 74 p.

Cramer, B.S., Wright, J.D., Kent, D.V., Aubry, M.-P., 2003. Orbital climate forcing of d13C excursions in the late Paleocene–early Eocene (chrons C24n–C25n). Paleoceanography 18 (4), 1097. doi:10.1029/2003PA000909.

Di Napoli Alliata, E., Proto Decima, F., Pellegrini, G.B., 1970. Studio Geologico, Stratigrafico e Micropaleontologico dei Dintorni di Belluno. Mem. Soc. Geol. Ital. 9, 1–28.

Dinarès-Turell, J., Baceta, J.I., Pujalte, V., Orue-Etxebarria, X., Bernaola, G., 2002. Magnetostratigraphic and cyclostratigraphic calibration of a prospective Paleocene/Eocene stratotype at Zumaia (Basque Basin, northern Spain). Terra Nova 14, 371–378.

Dinarès-Turell, J., Baceta, J.I., Pujalte, V., Orue-Etxebarria, X., Bernaola, G., Lorito, S., 2003. Untantling the Paleocene climatic rhythm: an astronomically calibrated Early Paleocene magnetostratigraphy and biostratigraphy at Zumaia (Basque Basin, northern Spain). Earth Planet. Sci. Lett. 216, 483–500.

Dinarès-Turell, J., Baceta, J.I., Bernaola, G., Orue-Etxebarria, X., Pujalte, V., 2007. Closing the Mid-Paleocene gap: toward a complete astronomically tuned Paleocene Epoch and Selandian and Thanetian GSSPs at Zumaia (Basque Basin, W Pyrenees). Earth Planet. Sci. Lett. 262, 450–467.

Doglioni, C., Bosellini, A., 1987. Eoalpine and meso-alpine tectonics in the Southern Alps. Geol. Rundsch. 77, 734–754.

Estes, R., Hutchison, J.H., 1980. Eocene lower vertebrates from Ellesmere Island, Canadian Arctic Archipelago. Palaeogeogr. Palaeoclimatol. Palaeoecol. 30, 325–347.

Gaetani, M., Jadoul, F., 1979. The structure of Bergamasc Alps. Rend. Azz. Naz. Lincei, 8, 66, 5, 411–416.

Gibbs, S.J., Bown, P.R., Sessa, J.A., Bralower, T.J., Wilson, P.A., 2006. Nannoplankton extinction and origination across the Paleocene–Eocene Thermal Maximum. Science 314, 1770–1773.

Giusberti, L., Rio, D., Agnini, C., Backman, J., Fornaciari, E., Tateo, F., Oddone, M., 2007. Mode and tempo of the Paleocene–Eocene thermal maximum in an expanded section from the Venetian pre-Alps. Geol. Soc. Amer. Bull. 119, 391–412. doi:10.1130/B25994.1.

Kennett, J.P., Stott, L.D., 1991. Abrupt deep-see warming, paleoceanographic changes and benthic extinctions at the end of the Paleocene. Nature 353, 225–229.
Kent, D.V., Olsen, P.E., Witte, W.K., 1995. Late Triassic–earliest Jurassic geomagnetic polarity sequence and paleolatitudes from drill cores in the Newark rift basin, eastern North America. J. Geo-phys. Res. 100, 14965–14998.
Kirschvink, J.L., 1980. The least-squares line and plane and analysis of paleomagnetic data. Geophys. J. R. Astron. Soc. 62, 699–718.
Lowrie, W., 1990. Identification of ferromagnetic minerals in a rock by coercivity and unblocking temperature properties. Geophys. Res. Lett. 17, 150–162.
Lowrie, W., Alvarez, W., 1977. Upper Cretaceous–Paleocene magnetic stratigraphy at Gubbio, Italy: III. Upper Cretaceous magnetic stratigraphy. Geol. Soc. Amer. Bull. 88, 374–377.
Lowrie, W., Alvarez, W., Napoleone, G., Perch-Nielsen, K., Premoli Silva, I., Toumarkine, M., 1982. Paleogene magnetic stratigraphy in Umbrian pelagic carbonate rocks: The Contessa sections, Gubbio. Geol. Soc. Amer. Bull. 93, 414–432.
Martini, E., 1971. Standard Tertiary and Quaternary calcareous nannoplankton zonation, In: Farinacci, A. (Ed.), Proceedings of the 2nd Planktonic Conference, 2, ed. Tecnoscienza, Roma, pp. 739–785.
McFadden, P.L., McElhinny, M.W., 1990. Classification of the reversal test in palaeomagnetism. Geophys. J. Int. 103, 725–729.
McKenna, M.C., 1980. Eocene paleolatitude, climate, and mammals of Ellesmere Island. Palaeogeogr. Palaeoclimatol. Palaeoecol. 30, 349–362.
Miller, K.G., Wright, J.D., Browning, J.V., 2005. Visions of ice sheets in a greenhouse world. Mar. Geol. 217, 215–231.
Monechi, S., Thierstein, H.R., 1985. Late Cretaceous–Eocene nannofossil and magnetostratigraphic correlations near Gubbio, Italy. Mar. Micropaleontol. 9, 419–440.
Moran, K., Backman, J., Brinkhuis, H., Clemens, S.C., Cronin, T., Dickens, G.R., Eynaud, F., Gattacceca, J., Jakobsson, M., Jordan, R.W., Kaminski, M., King, J., Koc, N., Krylov, A., Martinez, N., Matthiessen, J., McInroy, D., Moore, T.C., Onodera, J., O'Regan, M., Pälike, H., Rea, B., Rio, D., Sakamoto, T., Smith, D., Stein, R., St John, K., Suto, I., Suzuki, N., Takahashi, K., Watanabe, N., Yamamoto, M., Farrell, J., Frank, M., Kubik, P., Jokat, W., Kristoffersen, Y., 2006. The Cenozoic palaeoenvironment of the Arctic Ocean. Nature 441, 601–605.
Muttoni, G., Garzanti, E., Alfonsi, L., Cirilli, S., Germani, D., Lowrie, W., 2001. Motion of Africa and Adria since the Permian: paleomagnetic and paleoclimatic constraints form northern Libya. Earth Planet. Sci. Lett. 192, 159–174.
Muttoni, G., Kent, D.V., Garzanti, E., Brack, P., Abrahamsen, N., Gaetani, M., 2003. Early Permian Pangea "B" to Late Permian Pangea "A". Earth Planet. Sci. Lett. 215, 379–394.
Muttoni, G., Kent, D.V., Garzanti, E., Brack, P., Abrahamsen, N., Gaetani, M., 2004. Erratum to Early Permian Pangea "B" to Late Permian Pangea "A": [Earth Planet Sci. Lett. 215, 2003, 379–394]. Earth Planet. Sci. Lett. 218, 539–540.
Napoleone, G., Premoli, Silva, I., Heller, F., Cheli, P., Corezzi, S., Fischer, A.G., 1983. Eocene magnetic stratigraphy at Gubbio, Italy, and its implications for Paleogene geochronology. Geol. Soc. Amer. Bull. 94, 181–191.
Okada, H., Bukry, D., 1980. Supplementary modification and introduction of code numbers to the low-latitude coccolith biostratigraphic zonation (Bukry, 1973; 1975). Mar. Micropaleontol. 5, 321–325.
Perch-Nielsen, K., 1985. Cenozoic calcareous nannofossils. In: Bolli, H.M., et al. (Ed.), Plankton Stratigraphy. Cambridge University Press, New York, pp. 427–554.
Raffi, I., Backman, J., Pälike, H., 2005. Changes in calcareous nannofossil assemblage across the Paleocene/Eocene transition from the paleo-equatorial Pacific Ocean. Palaeogeogr. Palaeoclimatol. Palaeoecol. 226, 93–126.
Raffi, I., Backman, J., Fornaciari, E., Pälike, H., Rio, D., Lourens, L.J., Hilgen, F.J., 2006. A review of calcareous nannofossil astrobiochronology encompassing the past 25 Million years. Quat. Sci. Rev. 25, 3113–3137.
Rio, D., Raffi, I., Villa, G., 1990. Pliocene–Pleistocene calcareous nannofossil distribution patterns in the western Mediterranean. Proc. Ocean Drill. Prog. Sci. Results 107, 513–533.
Rosenbaum, G., Lister, G.S., Duboz, C., 2004. The Mesozoic and Cenozoic motion of Adria (central Mediterranean): a review of constraints and limitations. Geodin. Acta 17 (2), 125–139.
Singer, M.J., Verosub, K.L., Fine, P., TenPas, J., 1996. A conceptual model for the enhancement of magnetic susceptibility in soils. Quat. Int. 34–36, 243–248.
Sloan, L.C., Rea, D.K., 1995. Atmospheric carbon dioxide and early Eocene climate: a general circulation modeling sensitivity study. Palaeogeogr. Palaeoclimatol. Palaeoecol. 119 (3–4), 275–292.
Stefani, C., Grandesso, P., 1991. Studio preliminare di due sezioni del Flysch Bellunese. Rend. Soc. Geol. Ital. 14, 157–162.
Tauxe, L., Kent, D.V., 1984. Properties of detrital remanence carried by hematite from study of modern river deposits and laboratory redeposition experiments. Geophys. J. R. Astron. Soc. 76, 543–561.
Tauxe, L., Kodama, K.P., Kent, D.V., 2008. Testing corrections for paleomagnetic inclination error in sedimentary rocks: a comparative approach. Phys. Earth Planet. Int. 169, 152–165.
Walker, J.C.G., Hays, P.B., 1981. A negative feedback mechanism for the long-term stabilization of the Earth's surfaces temperature. J. Geophys. 86, 9776–9782.
Watson, G., 1983. Large sample theory of the Langevin distributions. J. Stat. Plan. Inference 8, 245–256.
Wilson, M.J., 2004. Weathering of the primary rock-forming minerals: processes, products and rates. Clay Miner. 39, 233–266.
Winterer, E.L., Bosellini, A., 1981. Subsidence and sedimentation on Jurassic passive continental margin, Southern Alps, Italy. Am. Assoc. Pet. Geol. Bull. 65, 394–421.
Wise, S.W., Breza, J.R., Harwood, D.M., Wei, W., 1991. Palaeogene glacial history of Antarctica. In: Mã œ llerIII III, D.W., McKenzie, J.A., Weissert, H. (Eds.), Controversies in Modern Geology: Evolution of Geological Theories in Sedimentology, Earth History and Tectonics. Academic Press, London, pp. 133–171.
Wolfe, J.A., 1980. Tertiary climates and floristic relationships at High latitudes in the northern hemisphere. Palaeogeogr. Palaeoclimatol. Palaeoecol. 30, 313–323.
Zachos, J.C., Stott, L.D., Lohmann, K.C., 1994. Evolution of marine temperatures during the Paleogene. Paleoceanography 9, 353–387.
Zachos, J., Pagani, M., Sloan, L., Thomas, E., Billups, K., 2001. Trends, rhythms and aberrations in global climate 65 Ma to present. Science 292, 686–693.
Zijderveld, J.D.A., 1967. A.C. demagnetization of rocks: analysis of results. In: Collinson, D.W., et al. (Ed.), Methods in Paleomagnetism. Elsevier, Amsterdam, pp. 254–286.